

Combined detection of nitrite and bioelectrical activity using microelectrode arrays and a phosphate buffered saline solution

F. L. Almeida^a, W. B. Souza Junior^a, Y. L. Moraes^a, S. G. dos Santos Filho^b, D. M. Veronez^c, I. A. Cestari^d
^aIndustrial Automation, Faculdade de Tecnologia de Itaquera ‘Professor Miguel Reale’ (Fatec Itaquera), Brazil

^bLSI/PSI/EPUSP, University of São Paulo, Brazil

^cPolytechnique School, Other University of São Paulo, Brazil

^dLaboratory of Bioengineering, Institute of the Heart (InCor), University of São Paulo, Brazil

fernando.almeida14@fatec.sp.gov.br wilmarjunior95@hotmail.com yann465@hotmail.com
sgsantos@lsi.usp.br dougveronez@gmail.com idagene.cestari@incor.usp.br

Abstract — This paper presents the manufacturing of a microelectrode array, on printed circuit boards (PCB) substrate (28.4 mm wide and 28.4 mm long), composed of 60 to 64 gold microelectrodes (between 4 μm and 70 μm each in diameter). The sensor has a measurement total area of 0.5 cm in radius, one gold-auxiliary electrode (GAE) of 1 mm² in area and one commercial AgAgCl (3 M NaCl) reference electrode from BASI®. These microelectrodes were used for checking and logging of extracellular local field potential of cell culture or cardiac tissue in a phosphate buffered saline (PBS) solution (stabilized-electrolytes aqueous medium and pH 7.4). In addition, an apparatus to shield from electromagnetic interference for connecting the arrays was designed to allow the capture of electrochemical or electronic signals by the microelectrodes, for example: nitrite (some Au-P1m-Cu(II)- μ -electrodes) or cardiac potential measurement (bare gold microelectrodes), respectively. Finally, biocompatibility tests of the array structures were performed. The preliminary electrical and biocompatibility testing, along with the collected data, has shown promising results pointing to the development of an accurate sensor after the completion of this study. The sensor has potentially a broader range of applications with only a few adaptations and due its good accuracy it can be a very useful resource for many chemical and biological applications; e.g., including the heart failure (HF).

Keywords: extracellular local field potentials, myoblasts, gold microelectrodes, nitrite, heart.

I. INTRODUCTION

Heart failure (HF) is the last and the most severe stage of various heart diseases and it is a progressive dilatation and dysfunction of myocardium [1]. According to data from the Hospital Information System (HIS) and Unified Health System (SUS), 82.591 hospital admittances were recorded in the first quarter of 2018 for circulatory diseases, among these, 13.945 cases were diagnosed with HF. This corresponds to 17 % of all admittances are associating with circulatory diseases in Brazil [2].

The definitive treatment is heart transplantation [1,3] for HF. The shortage of organs, however, leads 30 % of patients to death, according to the transplantation waiting list on priority basis in São Paulo for the period of 2002 to 2008 [3]. Statistics from 2017 of the Brazilian Transplant Registry shows that 380 transplants were performed in the last year and the waiting list still counted 291 active patients [4,5]. In this scenario, the myocardial reverse remodeling has been recently considered [6] and there is no clear understanding on

the mechanisms that lead to myocardial recovery [7,8]. It is only known that such recovery affects the heart muscle in metabolic, mechanical and electrophysiological terms [9-11]. Therefore, the combined study of the cardiac action potential for myocardial recovery can potentially disclose and expand the criteria for evaluation of the heart.

From the point of view of electrical activity, HF generates distortions mainly on morphology and duration of the action potentials. In addition, the calcium cycle also changes, which directly affects the contractile performance of the muscle. The action potential can be understood as a distinct and individual variation on the potential of membrane. These potentials come from excitations or disturbances from external areas to the cell and induce variations on the flow of ionic charges in the cell membrane region.

In the cardiac muscle, the action potential is generated by the opening of two types of channels: the fast sodium channels and the slow calcium channels (also called calcium-sodium channels). The slow calcium channels are an essential feature for the heart and remain opened for much longer than the fast sodium channels. This maintains the depolarization on the heart muscle for longer time intervals [12].

In addition to this effect, the potassium channels also act differently; right after the onset of the action potential, potassium channels have the permeability decreased by five times, which prevents the rapid repolarization of the membrane. The action potential ends only after about 0.2 s – 0.3 s, when the calcium-sodium channels are closed, and the permeability of potassium channels are back to normal performance [12]. This slow action potential also causes a very long refractory period of the heart muscle; it takes 0.2 s – 0.3 s. This time interval is almost identical to that of the action potential. It is worth noting an additional relative refractory period of 0.05 s [13].

The potential plateau and the refractory period are very important features for the proper working of the heart muscle. Considering the duration of the potential in skeletal muscle at 5 ms [12], a heart submitted to such rhythm would have a very high beat rate and inefficient blood pumping. For the blood to be pumped appropriately with gas exchange and not at a very high pressure, it is necessary a heart on slower and strong contractions.

The aim of this article is developing and testing a microelectrode array (sensors) on SU-8 polymer-coated printed circuit board (PCB) substrates to characterize entirely the electrophysiological behavior of cardiomyocytes [14-16]. These microelectrodes capture the electrical signals propagated through an electrolyte solution [17,18]. Also, it was investigated the use of electrochemical techniques for combined detection of nitrite ion (NO_2^-) [19,20], which are

associated with electrophysiological behavior on cardiac activity and human health [20]. The electrochemical techniques are less used for biochemical measurements in blood [21] possibly due to the great number of interfering chemical species and the poor sensitivity at reduced concentrations of nitrite in blood below 20 nmol cm^{-3} [22].

This work proposes an integrated system composed of the microelectrode arrays on SU-8 polymer-coated PCB substrate and shielded pack to avoid external electromagnetic interference and the biocompatible array of structures.

II. METHODOLOGY

A. Materials and Equipments

The materials and equipments used in this research were: a) five 50 mm chromium masks on glass to define the microelectrode arrays, and 30 SU-8 polymer-coated PCB substrates (28.4 mm wide and 28.4 mm long); b) reagents – photoresist SU-8 2002, SU-8 developer and PG remover from MicroChem NANO™; DIP gold 512 from Coimpa, Arguna® ET-S silver electrolyte and Auruna® 559 fine gold electrolyte from Umicore; 18 MΩ cm deionized water from MilliQ, iron perchlorate, imidazole, hydrogen peroxide, copper sulfate, sodium phosphate from Sigma-Aldrich; sulfuric acid (33 %), isopropyl alcohol (IPA) and acetone from Lab Alley; c) additional materials – tin wires, silicone adhesive, silicone o-ring (0.6 mm in radius and 1.8 cm in length), H9c2 myoblasts, Human Umbilical Vein Endothelial Cells (HUVEC), C2041206P2 gold paste from Gwent Electronic Materials Ltd.; and d) equipments and softwares – manual diamond-tipped glass cutter, screw drivers, soldering iron, AutoCAD and LabView softwares, CNC machining center, 3-D printer (Object 3D Pro from Strasys), Autolab PGSTAT302N and Nova 1.9 software.

B. Techniques and Methods

The methods and techniques applied during the design development were: a) cutting of PCB boards using a computerized numerical control (CNC) machining center; b) photo-etching by wet-etching (preparation of copper / arrays); c) chemical deposition of silver and gold (on copper to obtain the gold microelectrodes); d) additive fabrication (apparatus for connecting the microelectrode array via 3-D printing); e) potentiometry (for the analyze of cardiac potential stimuli); f) cyclic voltammogram (CV) for nitrite measurement; and g) cell cultivation (for biocompatibility testing).

C. Fabrication of the Integrated System (IS)

The IS was fabricated as follows [23-25]:

- i) Microelectrode arrays and shielded apparatus were designing per AutoCAD software;
- ii) Copper metallized-PCB substrates (1.6 mm or 0.8 mm thick) were cutting at dimensions of 28.4 mm x 28.4 mm;
- iii) Photoresist SU-8 2002 from MicroChem NANO™ at (2 – 5) μm thick was depositing;
- iv) Sensor structures were transferring to the PCB substrates using a photolithographic aligner;
- v) The corrosion of the exposed copper was performing with an iron perchlorate solution;
- vi) SU-8 photoresist was removing by PG Remover;

- vii) A gold film ($< 100 \mu\text{m}$) on the copper metallized-PCB substrate was chemically depositing;
- viii) SU-8 photoresist was placing to coat the PCB substrate;
- ix) A new photolithograph was employing to expose the gold microelectrodes (4-70 μm in diameter), and gold-auxiliary-electrode (GAE) with area of 1 mm^2 was also defining;
- x) Gold- μ electrode surfaces were electrochemically changing with imidazole and functionalize it with copper (II);
- xi) Biocompatibility tests were performing; and
- xii) Electrical validation of the arrays was analyzing.

III. DEVELOPMENT

A. Microelectrode Arrays

Microelectrode arrays are devices for detecting electrical signals constituted by a treated substrate containing uniformly distributed small electrodes. In addition to the electrodes, the substrate also has conductive structures responsible for carrying the measured signals to points of connection with the data acquisition system. Using the microelectrode arrays, it was possible to study the electrical activity of biological samples properly positioned on the measurement area (see black circle in Fig. 1).

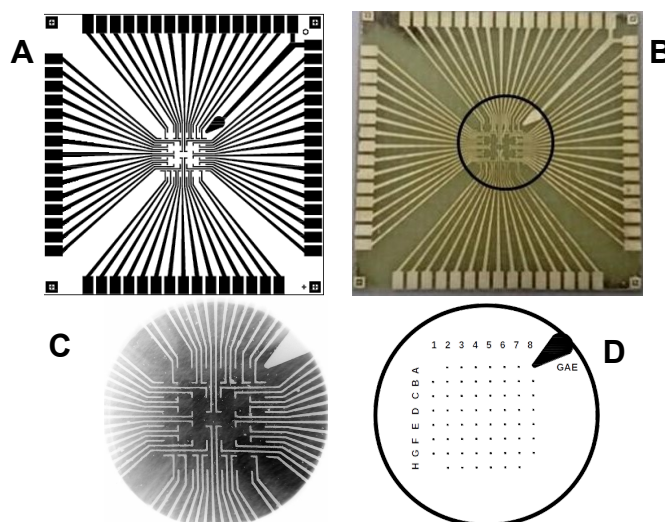


Fig. 1. (a) masks design; (b) SU-8-coated PCB substrate with gold-deposited over copper; (c) optical image detail of the arrays; and (d) measurement window with 60 gold microelectrodes ($\sim 25 \mu\text{m}$ in radius) and gold-auxiliary electrode (GAE) of 1 mm^2 in area. Source: authors.

The dimensions of the microelectrode arrays (sensor), particularly the measurement area and their contacts, are presenting in Tab. 1.

Tab. 1. Features of the microelectrode arrays.

Descriptions	Dimensions
Microelectrodes (diameter)	4 to 70 μm
distance between microelectrodes (center to center)	600 μm
gold-auxiliary electrode (area)	1 mm^2
active region	4.25 mm
measuring window	10 mm
sensor substrate (PCB)	28.4 mm x 28.4 mm
each contact pad	1 mm
amount of microelectrode	60

Source: authors.

The preparation of the microelectrode arrays was performing by traditional lithographic techniques. In the following, it is presenting the steps and parameters used in the deposition, photolithography, development and removal of SU-8:

- i. SU-8 4 μm -deposition:
speed = 3000 rpm;
ramp = 500 rpm s⁻¹; and
time = 30 s.
- ii. photoengraving:
pre-cure: $(95 \pm 0.5)^\circ\text{C}$ for 3 min;
UV exposure: 35 s. (the contact force of the aligner should be adjusted to 1.3); and
cure: $(95 \pm 0.5)^\circ\text{C}$ during 3 min;
- iii. development: 35 s in SU-8 developer;
- iv. chemical cleaning in IPA, to remove white regions due to not removed SU-8 traces;
- v. corrosion of the exposed copper with iron perchlorate solution for 85 min;
- vi. removal of SU-8 with MicroChem PG Remover at 80°C for 15 min;
- vii. cleaning with 'piranha' solution diluted at room temperature, i.e., 3:1:1, deionized water, hydrogen peroxide and sulfuric acid (33 %) for 3 min;
- viii. chemical deposition of silver using Arguna solution at 80°C for 30 s; and
- ix. chemical deposition of gold (Coimpa gold DIP 512) at 80°C for 150 min.

B. Shielded Apparatus

The shielded apparatus contains connectors and supporting structures where the microelectrode arrays are docking. In this way, they connect to the signal acquisition equipment and positioned on inverted microscopes. The metal parts of the shielded apparatus had been machined and mounted on plastic parts produced by 3-D printing. The apparatus was manufacturing at dimensions listed in Tab. 2.

Tab. 2. Dimensions of apparatus for mounting arrays.

Descriptions	Measures
maximum height:	between 20 and 25 mm
radius of the preview window	greater than 15 mm
width	50 mm
length	50 mm
O-ring	15 mm i.d. and 20 mm o.d.

Source: authors.

Fig. 2 shows 3-D view apparatus to connect the microelectrode arrays, drawn with aid of the AutoCAD software. The parts of the 3-D exploded view are:

- i) base of the microelectrode array;
- ii) contra base to connect in the packing structure;
- iii) apparatus structure that envelop the golden pins for connection on sensor pads;
- iv) board with the golden pins; and
- v) the cover with a fixing plate.

Note: the biological material grow directly on the sensor measurement region; thus, one can extract physiological parameters.

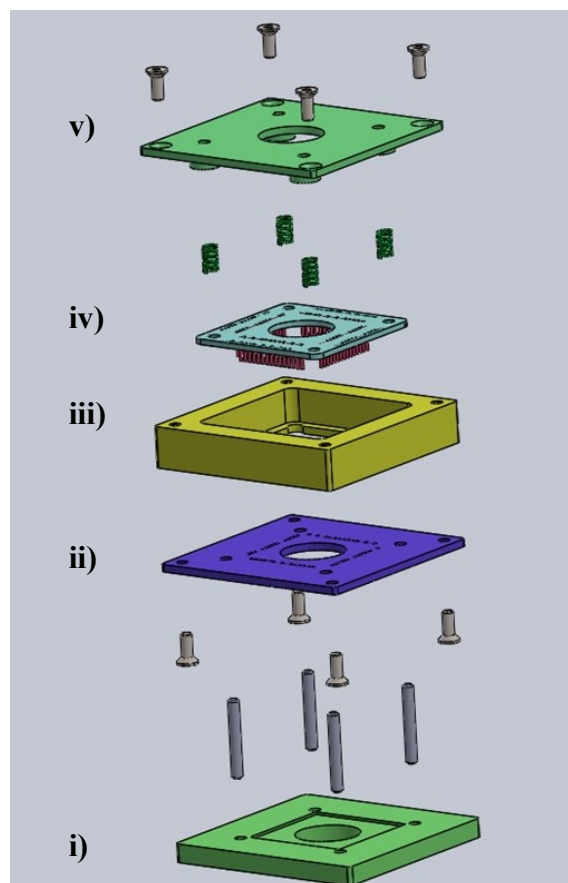


Fig. 2. 3-D view of the machined apparatus for connecting the microelectrodes. Source: authors.

Some changes in the apparatus connecting and the protection case against electromagnetic interference were implementing. The result was a new connection apparatus with golden pins and nickel-plated copper mesh wrapped in flat cables (Fig. 3). Also, at the end of the flat cable, there is the new protection case (rigid, nickel-plated and braided mesh) in the region of the DB-25 connector.



Fig. 3. Supporting apparatus to connect the array and to measure the potentials, and electromagnetic shielding. Source: authors.

Fig. 4 shows the apparatus' base and top for connecting the microelectrode arrays.

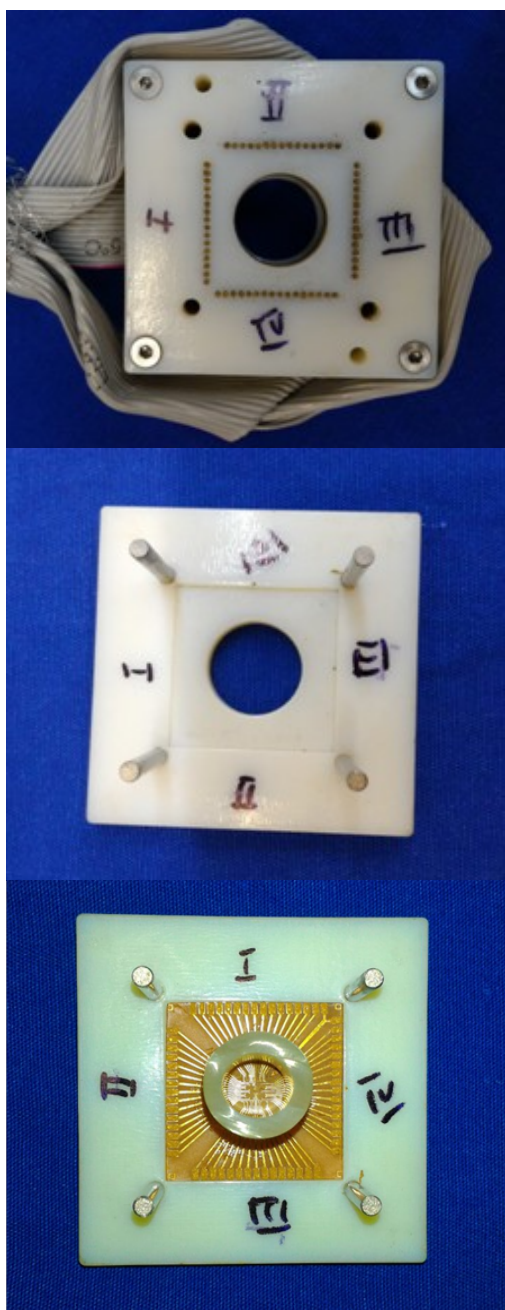


Fig. 4. Details of the apparatus for connection of microelectrode arrays.
Source: authors.

On a microelectrode array, there is a silicone O-ring attached, like O-ring's Multichannel Systems, which allows to introduce aqueous solution and biological materials.

C. Biocompatibility Testing

The microelectrode arrays are useful for evaluating the electrical activity of biological material, so it is important that the materials used in its manufacturing are non-toxic or induce physiological responses in the cells and electrolytes under study.

The biocompatibility tests make it possible to verify if the materials used in the prototype production process of the microelectrode arrays and the shielded measuring apparatus are suitable. To accomplish these, myoblasts (H9c2) and endothelial cells HUVEC had been cultured according to the following protocols.

H9c2 myoblasts were growing in T75 flasks with Dulbecco's Modified Eagle's Medium (DMEM) supplemented with 10 % (v/v) fetal bovine serum and 1 % (v/v) penicillin / streptomycin in an atmosphere saturated with water at 5 % CO₂ at 37 °C to reach approximately 80 % confluence. Endothelial cells HUVEC were growing and collecting in similar conditions, but the culture medium used was RPMI supplemented with 10 % (v/v) fetal bovine serum and 1 % (v/v) penicillin/streptomycin.

For biocompatibility tests, the cells were collecting in trypsin 0.25 % EDTA solution and plated on 35 mm dishes containing the materials used to manufacture the microelectrode arrays. After 24 hours of plating, the cultures were observing under a microscope.

Dishes containing toxic materials showed large numbers of dead cells, absence of cell adhesion or proliferation in relation to the controls.

D. Electrical Testing of Microelectrodes

Two electrical tests were conducting on the arrays. The first was intending to measure the ability of the electrodes to transmit the stimulus to phosphate buffered saline (PBS) solution, that is a stabilized-electrolytes aqueous medium and pH 7.4 simulated by CHEAQS Pro Release P2013.1 [24]. It was employing as a control solution to obtain the background signals. The second measured the ability of the electrode to record the propagation of a stimulus through PBS.

In the first test, an electrical stimulator (ES) was connecting to the microelectrode under analysis and the oscilloscope probe was placing in the center of the detection region to record the electrical signals transmitted to the PBS electrolytic solution (Fig. 5a).

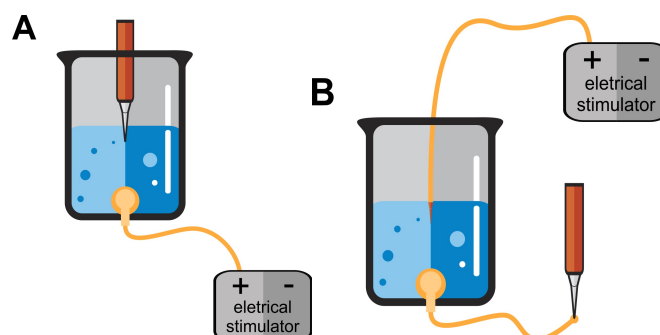


Fig. 5. Electrical stimulation on microelectrode measuring by solution (a) and in the solution mensuration by microelectrode (b). Source: authors.

In the second test, the ES was connecting to a probe so that pacing pulses were delivering to the solution present in the array through it and the oscilloscope probe was placing on pads connected to the other electrodes under analysis to record the electrical signals.

The stimulus signal used in the testing was a monophasic square pulse with duration of 5 ms and amplitude of 9 V.

E. Logging in the Acquisition System

To verify the performance of microelectrodes in recording small amplitude signals, the shielded integrated system was connecting to a multichannel acquisition system [25]. A new experimental setup was using in which a 400 mV of pulse at a 100 ms amplitude and 2 Hz frequency was applying to the solution from an electrode.

The signal captured by the other electrodes was recording by the acquisition system.

IV. RESULTS AND DISCUSSIONS

A. Biocompatibility Testing

Fig. 6 shows the 35 mm-dishes on which cells were plating and they were observing in an inverted optical microscope. In the Fig. 6a on the left, it is possible to identify a monolayer of cells adhered on the SU-8 polymer-coated substrate. The cells were well developing on the culture surface dish and on the treated glass indicating lack of toxicity in the materials. In the Fig. 6b on the right, on the disk containing the phenolite, there are no cells adhered.

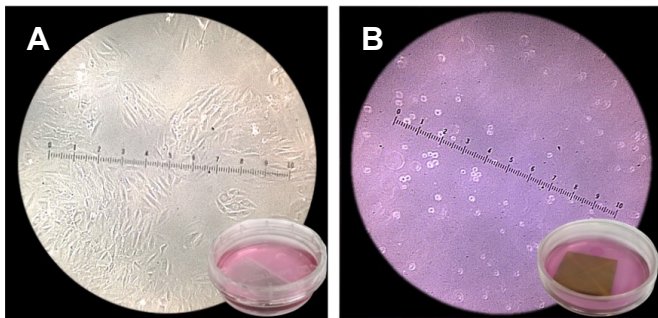


Fig. 6. Array material testing: a) SU-8 polymer; and b) only PCB. Source: authors.

On the other hand, dead cells had been observed floating in the solution, which indicates toxicity of the materials from arrays. SU-8 polymer showed suitable biocompatibility.

B. Results of the Electrical Testing

The map in Fig. 7 illustrates the signals transmitted to the solution from some gold microelectrodes of the array. We observed that the signal shape and duration (5 ms) were preserving, but the amplitude has varied widely. It is worth noting transmitted signals $[(3.50 \pm 0.81) \text{ V}]$ from electrodes to solution represent a 38 % charge transfer factor.

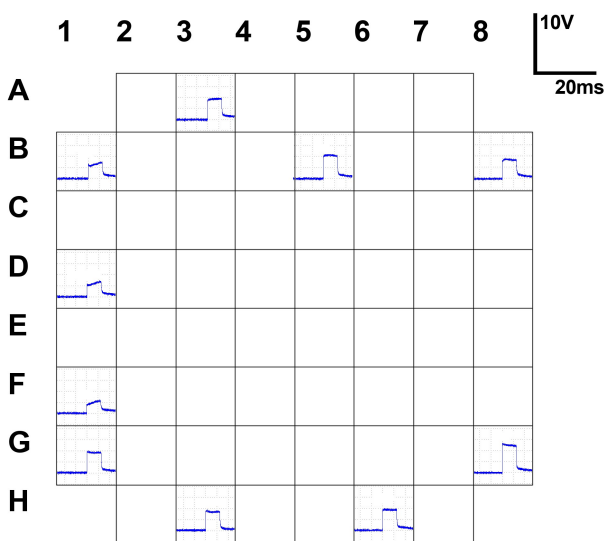


Fig. 7. Array scheme indicating the measured electrical signals between the PBS solution and some electrodes, randomly selected. Source: authors.

Tabs. 3 and 4 show measured voltage values between the PBS solution (ES) and the microelectrodes (Fig. 7) or C-8 microelectrode as ES (Fig. 8).

Tab. 3. The applied reference voltage was 9 V, and measured values on microelectrodes are described in table.

		Measured voltage on microelectrodes (V)							
		1	2	3	4	5	6	7	8
A	-	-	-	3.67	-	-	-	-	-
B	3.67	-	-	-	-	4.17	-	-	3.42
C	-	-	-	-	-	-	-	-	-
D	2.41	-	-	-	-	-	-	-	-
E	-	-	-	-	-	-	-	-	-
F	2.00	-	-	-	-	-	-	-	-
G	3.65	-	-	-	-	-	-	-	4.91
H	-	-	3.37	-	-	-	3.71	-	-

Source: authors.

To assess the ability of logging an electrical potential in the solution, electrodes were selecting with impedances ranging from the best to the worst scenario identified (9 MΩ to 95 MΩ). A 9 V-square pulse at 5 ms duration was applying across the electrode shown in red (Fig. 8). This signal was logging by the other electrodes.

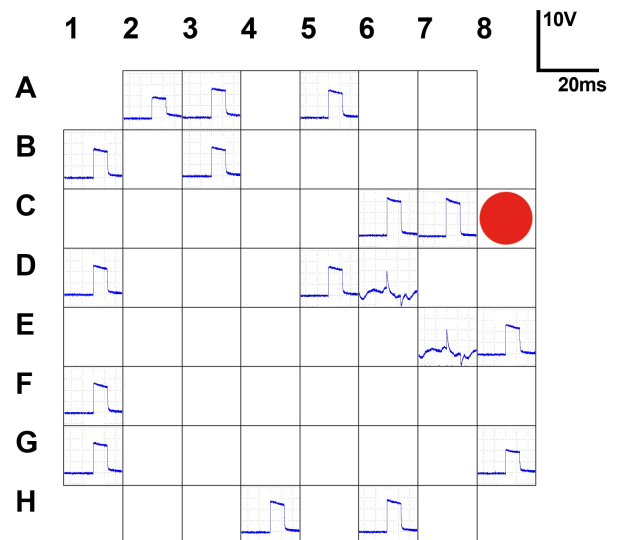


Fig. 8. Array scheme showing the signals measured by the microelectrodes in response to a stimulus given by the C-8 microelectrode. Source: authors.

Tab. 4. The applied reference voltage was also 9 V, and signals were recorded between the electrode C-8 and other microelectrodes.

		Recorded voltage by microelectrodes (V)							
		1	2	3	4	5	6	7	8
A	-	3.71	5.02	-	4.91	-	-	-	-
B	4.91	-	4.91	-	-	-	-	-	-
C	-	-	-	-	-	-	6.17	6.22	stim
D	4.91	-	-	-	4.91	interf	-	-	-
E	-	-	-	-	-	-	interf	4.97	-
F	4.91	-	-	-	-	-	-	-	-
G	5.08	-	-	-	-	-	-	-	3.94
H	-	-	-	5.14	-	5.31	-	-	-

Source: authors.

On average, the electrodes logged a 5 ms of duration pulse at $(5.00 \pm 0.64) \text{ V}$ in amplitude. The amplitude of the logged signal is as high as the measured signals in the solution, indicating a very low charge loss in the acquisition of potential.

The manufactured bare gold microelectrodes were able to capture the potentials in the solution. With respect to stimulation, losses are usually high and vary with the material. Gold is a good solution to compromise between stimulation and acquisition.

Tab. 5 show impedance values between the microelectrodes and the respective pads.

Tab. 5. Resistance of the microelectrodes used to record the signals applied to the solution by the microelectrode C-8.

Resistance measured from each microelectrode (MΩ)								
	1	2	3	4	5	6	7	8
A	-	22	14	-	32	-	-	-
B	9	-	25	-	-	-	-	-
C	-	-	-	-	-	9	10	stim
D	12	-	-	-	24	40	-	-
E	-	-	-	-	-	-	95	10
F	18	-	-	-	-	-	-	-
G	12	-	-	-	-	-	-	11
H	-	-	-	16	-	15	-	-

Source: authors.

The average impedance of the electrodes was (22 ± 21) MΩ, the deviation is as high as the average, which indicates a wide variation in values. These results motivated us to rework the electrodes for standardizing their impedance. This directly affects the uniformity of charge transfer for logging and stimulation and it is desirable that the electrodes have a similar behavior.

We found that electrodes at impedance higher than 40 MΩ are not capable of logging signals, acting as coupling capacitances, which block DC signals.

After reworking the array to improve the electrodes and the coupling at the connection step, the average impedance fell to (12 ± 4) MΩ. The impedances not only decreased but also became more uniform along the array. The capacity of charge transferring of the solution and potential logging was not changed.

C. Acquisition of the Electrical Potentials

Fig. 9 shows the signal logged in H-6 a gold microelectrode from the acquisition system with a 1 kHz-sampling frequency. The extracellular local field potential was filtering to remove the 60 Hz electrical and thermal noises. It is possible to note that there is noise in the signal detected. As they are signals of high impedance, the connection with the acquisition system and distance of the cables can introduce noise on the millivolt ranges [14].

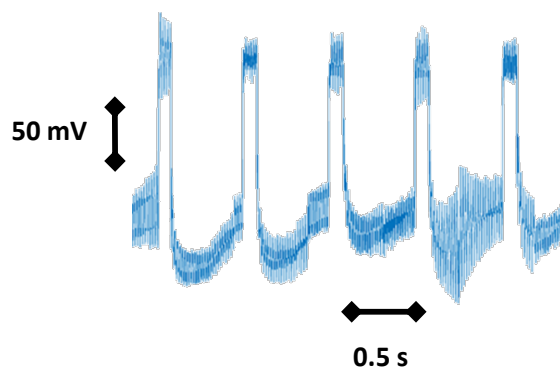


Fig. 9. Bioelectrical activity in PBS using H-6 gold microelectrode, electrical stimulation pulses at +150 mV in relation to the GAE (multi-channel acquisition system). Source: authors.

D. Nitrite's Bioelectrical Activity

Fig. 10(a) shows the CV nitrite measurements using 1:1 dilution of porcine blood in PBS and three interconnected Au-PIm-Cu(II)-μelectrodes (A-2, A-3 and B-3, for example). As observed in Fig. 10(b), which is a magnification of Fig. 10(a), the highest sensitivity for chemical species ligated to the transition metals [26-30]. In this work, the nitrite ligated to the copper (II) was detected around a reduced potential of +50 mV_{Ag/AgCl} 3M NaCl [31] and the lowest influence of the interfering-chemicals was also around this potential [24,32,33]. From the planar microelectrode theory and electrochemical techniques [34,35], Fig. 10(c) shows the limit currents at the highest sensitivity as a function of the nitrite concentrations above Cu(II)-poly(imidazole) film. For more positive potentials, there is a little change of the anodic current due to exclusive contribution of the free nitrite oxidation [31] at a +300 mV_{Ag/AgCl} 3M NaCl potential [24] and there is an increase substantially of the anodic current for upper potentials [26,33]. The limit current is relating to the individual microelectrode behavior (hemispherical diffusion), i.e., if d/r ratio ≥ 40 , anodic and cathodic peaks are converting in the limit current (d is the center-to-center distance between microelectrodes and r is the microelectrode radius) [33]. The oblique-asymptote-sigmoidal shape may be mixed to the capacitive and solution resistance effects on the polymeric membrane as a background response [36], which is adding to an expressive cathodic current for interconnected microelectrodes [37].

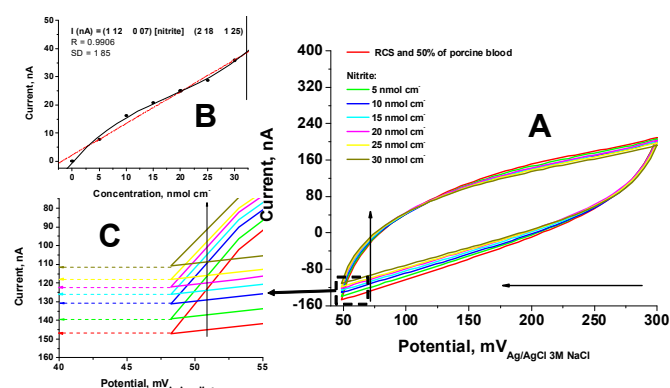


Fig. 10. (a) CV nitrite measurements using 1:1 dilution of porcine blood in PBS and three interconnected Au-PIm-Cu(II)-μelectrodes, (b) calibration curve, (c) detail of the measured current for nitrite concentrations above Cu(II)-poly(imidazole) film. Source: authors.

Thus, as depicted in Fig. 10(b), it is possible to detect nitrite with a sensitivity of $1.8 \cdot 10^5$ A mol⁻¹ cm using three Au-PIm-Cu(II)-μelectrodes with total effective area of (618.8 ± 70.0) μm² and a commercial Ag/AgCl (3M NaCl) reference electrode from BASi®. In addition to acquisition of the electrical potentials for cardiac applications, the nitrite was detected in vitro at very low concentrations. Gold-poly(imidazole)-μelectrodes were functionalizing with copper (II) and lower potentials were employing at pH 7.4.

V. CONCLUSIONS

This paper shown important results of the fabrication of microelectrode arrays for evaluating the electrical activity of cardiac cell cultures and of the measurement nitrite.

The electrical testing presented a good capacity for stimulation and logging of electrical potentials by the gold

microelectrode array, the impedances are quite uniform and most electrodes (90 %) worked properly. The bare gold microelectrodes had been used to record electrical pulses applied on an electrolytic aqueous medium.

The results obtained suggest the possibility of using the bare gold microelectrodes combined with three interconnected Au-PIIm-Cu(II)- μ electrodes to record extracellular field potentials and measure the nitrite ions, respectively. In this way, the treatment of heart failure (HF) can be monitored.

ACKNOWLEDGMENT

The authors thank the Brazilian National Council of Technological and Scientific Development (CNPq) and São Paulo Research Foundation (FAPESP), for the financial support.

FUTURE WORKS

The photolithography of microelectrode arrays on PCB with subsequent deposition of gold on copper needs additional tests. Thus, we intend to fine-tune the parameters for the fabrication of arrays in series using microelectrodes.

The integration between combined detection of nitrite and bioelectrical activity (extracellular local field potential) using an array of Au-PIIm-Cu(II)- μ electrodes will also be improved.

REFERENCES

- [1] F. Bacal et al. II Diretriz Brasileira de Transplante Cardíaco. *Arq Bras Cardiol.*, Vol. 94. No. 1 supl.1, pp. E16-E73, 2009. Available at: <http://www.scielo.br/pdf/abc/v94n1s1/01.pdf>. Accessed on: 27 May 2018.
- [2] Datasus. Morbidity SUS Hospital. Available at: <http://tabnet.datasus.gov.br/cgi/tabcgi.exe?sih/cnv/niuf.def>. Accessed on: 27 May 2018.
- [3] AI. Fiorelli. Hospital mortality in waiting list for heart transplantation: a comparative analysis of patients operated as priority or not. In: VI BRAZILIAN CONGRESS OF HEART FAILURE. Available at: <http://congresso.cardiol.br/geic/viii/temaslivres/TLp16746.pdf>. Accessed on: 05 June 2015.
- [4] Registration Brazilian Transplant. ABTO. Available at: <http://www.abto.org.br/abtov03/default.aspx?mn=457&c=900&s=0>. Accessed on: 27 May 2018.
- [5] Registration Brazilian Transplant. Dimensionamento dos Transplantes no Brasil em cada estado. 2017. 117 p. Available at: <http://www.abto.org.br/abtov03/Upload/file/RBT/2017/rbt-imprensa-leitura-compressed.pdf>. Accessed on: 27 May 2018.
- [6] S. Klotz, J. Danser AH, and D. Burkhoff. Impact of left ventricular assist device (LVAD) support on the reverse cardiac remodeling process. *Prog. Biophys Mol. Biol.*, Vol. 97, No. 2-3, pp. 479-496, 2008. doi:10.1016/j.pbiomolbio.2008.02.002.
- [7] AV. Ambardekar, and MW. Buttrick. Reverse left ventricular remodeling with assist devices: a review of clinical, cellular and molecular effects. *Circ. Heart Fail.*, Vol. 4, No. 2, pp. 224-233, 2011. doi:10.1161/CIRCHEARTFAILURE.110.959684.
- [8] MH. Yacoub, and CM. Terracciano. The Holy Grail of LVAD-induced reversal of severe chronic heart failure: the need for integration. *European Heart Journal*, Vol. 32, No. 9, pp. 1052-1054, 2011. doi:10.1093/eurheartj/ehq503.
- [9] K. Dipla, JA. Mattiello, and V. Jeevanandam. Myocyte recovery after mechanical circulatory support in humans with end-stage heart failure. *Circulation*, Vol. 97, No. 23, pp. 2316-2322, 1998. doi:10.1161/01.CIR.97.23.2316.
- [10] PM. Heerdt, S. Klotz, and D. Burkhoff. Cardiomyopathic etiology and SERCA2a mechanical support during reverse remodeling of the failing human heart. *Anesth. Analg.*, Vol. 102, No. 1, pp. 32-37, 2006. doi:10.1213/01.ane.0000183642.09435.ad.
- [11] SG. Drakos et al.. Reverse Electrophysiologic remodeling after cardiac mechanical unloading for endstage nonischemic cardiomyopathy. *Ann. Thorac. Surg.*, Vol. 91, No. 1, pp. 764-769, 2011. doi:10.1016/j.athoracsur.2010.10.091.
- [12] AC. Guyton, and JE. Hall. *Tratado de Fisiologia Médica*, 12. ed. Elsevier, 2011. pp. 45-163.
- [13] E. Widmaier, H. Raff, and K. Strang. *Vander Vander's human physiology: the mechanisms of body function*. The McGraw-Hill Company, 2001.
- [14] P. Camelliti, A-SS. Abou, and RT. Smolenski. Adult human heart slices are a multicellular system suitable for electrophysiological and pharmacological studies. *Journal of Molecular and Cellular Cardiology*, Vol. 51, No. 3, pp. 390-398, 2011. doi:10.1016/j.yjmcc.2011.06.018.
- [15] A. Bussek et al.. Tissue Slices from Adult Mammalian Hearts as a Model for Pharmacological Drug Testing. *Cellular Physiology and Biochemistry*, Vol. 24, No. 5-6, pp. 527-536, 2009. doi:10.1159/000257528.
- [16] Carl Gold; Darrell A. Henze; Christof Koch. Using extracellular action potential recordings to constrain compartmental models. *J. Comput. Neur.*, Vol. 23, No. 1, pp. 39-58, 2007. doi:10.1007/s10827-006-0018-2.
- [17] LGJ. Tertoolen, SR. Braam, and BJ. Van Meer. Interpretation of field potentials measured on a multi electrode array in pharmacological toxicity screening on primary and human pluripotent stem cell-derived cardiomyocytes. *Biochem. and Biophys. Research Comm.*, Vol. 497, No. 4, pp. 1135-1141, 2018. doi:10.1016/j.bbrc.2017.01.151.
- [18] CB. Vidor. Teste e caracterização de uma matriz multieletrodo para registro de sinais eletrofisiológicos in vitro, 2012. 77 p. Universidade Católica do Rio Grande do Sul.
- [19] M. Zhang, F. Cheng, and F. Gan. Electrochemical nitrite nanosensor based on Au nanoparticles/graphene nanocomposites. *Int. J. Electrochem. Sci.*, Vol. 10, pp. 5905-5913, 2015. Available at: <http://or.nsf.gov.cn/handle/00001903-5/212867>. Accessed on: 20 Agu. 2018.
- [20] M. Habermeyer et al.. Nitrate and nitrite in the diet: How to assess their benefit and risk for human health. *Mol. Nutr. Food Res.*, Vol. 59, No. 1, pp. 106-128, 2015. doi:10.1002/mnfr.201400286.
- [21] MJ. Moorcroft, J. Davis, and RG. Compton. Detection and determination of nitrate and nitrite: a review. *Talanta*, Vol. 54, No. 5, pp. 785-803, 2001. doi:10.1016/S0039-9140(01)00323-X.

- [22] A. Dejam et al.. Erythrocytes are the major intravascular storage sites of nitrite in human blood. *Blood*, Vol. 106, No. 2, pp. 734-739, 2005. doi:10.1182/blood-200502-0567.
- [23] MBA. Sources, R. Furlan, and IA. Cestari. Microelectrode array is Potential Cardiac Mapping. IN: XVI International Conference on MICROELECTRONICS PACKAGING AND-SBMICRO2011. Pirenópolis, GO, Brazil, 2011.
- [24] FL. Almeida. Measurement microelectrodes Pim-Au-Cu (II) and solid state reference electrodes of Au / AuxCly / PPI-CI / PU: voltammetric sensor integrated on a planar substrate modified with silicon and conductive polymers for measuring in physiological medium of nitrite..., 2014. 332 p. Ph.D Thesis - Polytechnic School, University of São Paulo, São Paulo, Mar. 2014.
- [25] M. Mazzetto et al.. System detection, amplification and acquisition of potential for analysis of cardiac electrical activity. *J. Biom. Eng.*, Vol. 13, pp. 19-29, 1997.
- [26] JRC. Rocha, L. Kosminsky, TRLC. Paixão and M. Bertotti. Anodic oxidation of nitrite at a molybdenum oxide layer. *Electroanalysis*, Vol. 13, No. 2, pp. 155-160, 2001.
- [27] J. Davis, MJ. Moorcroft, SJ. Wilkins, RG. Compton and MF. Cardosi. Electrochemical detection of nitrate and nitrite at a copper modified electrode. *Analyst*, Vol. 125, No. 4, pp. 737-742, 2000.
- [28] R. Ojani, JB. Raoof and E. Zarei. Electrocatalytic Reduction of Nitrite Using Ferricyanide; Application for Its Simple and Selective Determination. *Electrochimica Acta*, Vol. 52, No. 3, pp. 753-759, 2006.
- [29] W-Y. Ko, W-H. Chen, C-Y. Cheng and K-J. Lin. Highly electrocatalytic reduction of nitrite ions on a copper nanoparticles thin film. *Sensors and Actuators B*, Vol. 137, No. 2, pp. 437-441, 2009.
- [30] MG. Almeida, A. Serra, CM. Silveira and JGG. Moura. Nitrite Biosensing via Selective Enzymes—A Long but Promising Route. *Sensors*, Vol. 10, No. 12, pp. 11530-11555, 2010.
- [31] FL. Almeida, SG dos Santos-Filho. Array of Cu(II)-PIm-Au microelectrodes for nitrite measurement, in IEEE 9th IberoAmerican Congress on Sensors, Bogota, Colombia, Nov. 2014, pages 1-4.
- [32] FL. Almeida and MBA. Fontes. Influence of the Interferers in the Nitrite Detection By using Planar Electrochemical Sensors. *ECS Transactions*, Vol. 9, No. 1, pp. 545-552, 2007. doi:10.1149/1.2766928.
- [33] FL. Almeida and SG. Santos-Filho. Nitrite Detection in Near-Neutral-pH Electrolytes by Differential Pulse Voltammetry Under Cross Interference of Uric Acid, Ascorbic Acid, and Paracetamol. *IEEE Sensors Letters*, Vol. 3, No. 3, pp. 1-4, 2019. doi:10.1109/LSSENS.2019.2897715.
- [34] CG. Zoski. *Handbook of Electrochemistry*, 5th ed. - Ch. 10 Microelectrode Arrays from S. Szunerits and L. Thouin, Oxford: UK, Elsevier, 2007. ISBN-13: 978-0-444-51958-0.
- [35] M. Lovrić. Differential Pulse Voltammetry on Spherical Microelectrodes. *Electroanalysis*, Vol. 11, No. 15, pp. 1089-, 1999.
- [36] C. Amatore, A. Oleinick and I. Svir. Capacitive and Solution Resistance Effects on Voltammetric Responses of a Thin Redox Layer Attached to Disk Microelectrodes. *Analytical Chemistry*, Vol. 80, No. 21, pp. 7957-7963, 2008. doi:10.1021/ac8012972.
- [37] X. Xie et al.. Development of an ultramicroelectrode arrays (UMEAs) sensor for trace heavy metal measurement in water. *Sensors and Actuators B*, vol. 97, pp. 168-173, 2004. doi:10.1016/j.snb.2003.08.012.